Supplementary Information

Generation of programmable dynamic flow patterns in microfluidics using audio signals

Peter Thurgood [1,†], Gianmarco Concilia [1], Nhiem Tran [2], Ngan Nguyen [1], Adam J. Hawke [1], Elena Pirogova [1], Aaron R. Jex [3, 4], Karlheinz Peter [5, 6], Sara Baratchi [7, *, †], Khashayar Khoshmanesh [1,*, †]

[1] School of Engineering, RMIT University, Melbourne, Victoria, Australia

[2] School of Science, RMIT University, Melbourne, Victoria, Australia

[3] Population Health and Immunity Division, The Walter and Eliza Hall Institute of Medical Research, Parkville, Victoria, Australia

[4] Faculty of Veterinary and Agricultural Sciences, The University of Melbourne, Parkville, Victoria, Australia

[5] Baker Heart and Diabetes Institute, Melbourne, Victoria, Australia

[6] Department of Cardiometabolic Health, The University of Melbourne, Parkville, Victoria, Australia

[7] School of Health & Biomedical Sciences, RMIT University, Bundoora, Victoria, Australia

† Corresponding authors:

Peter Thurgood: peter.thurgood@rmit.edu.au

Khashayar Khoshmanesh: khashayar.khoshmanesh@rmit.edu.au

Sara Baratchi: sara.baratchi@rmit.edu.au

* There authors contributed equally to this work.

Keywords: microfluidics, dynamic flow patterns, acoustic signals, music signals, smartphone

Supplementary information 1: Geometrical details of the microfluidic flow focusing structures

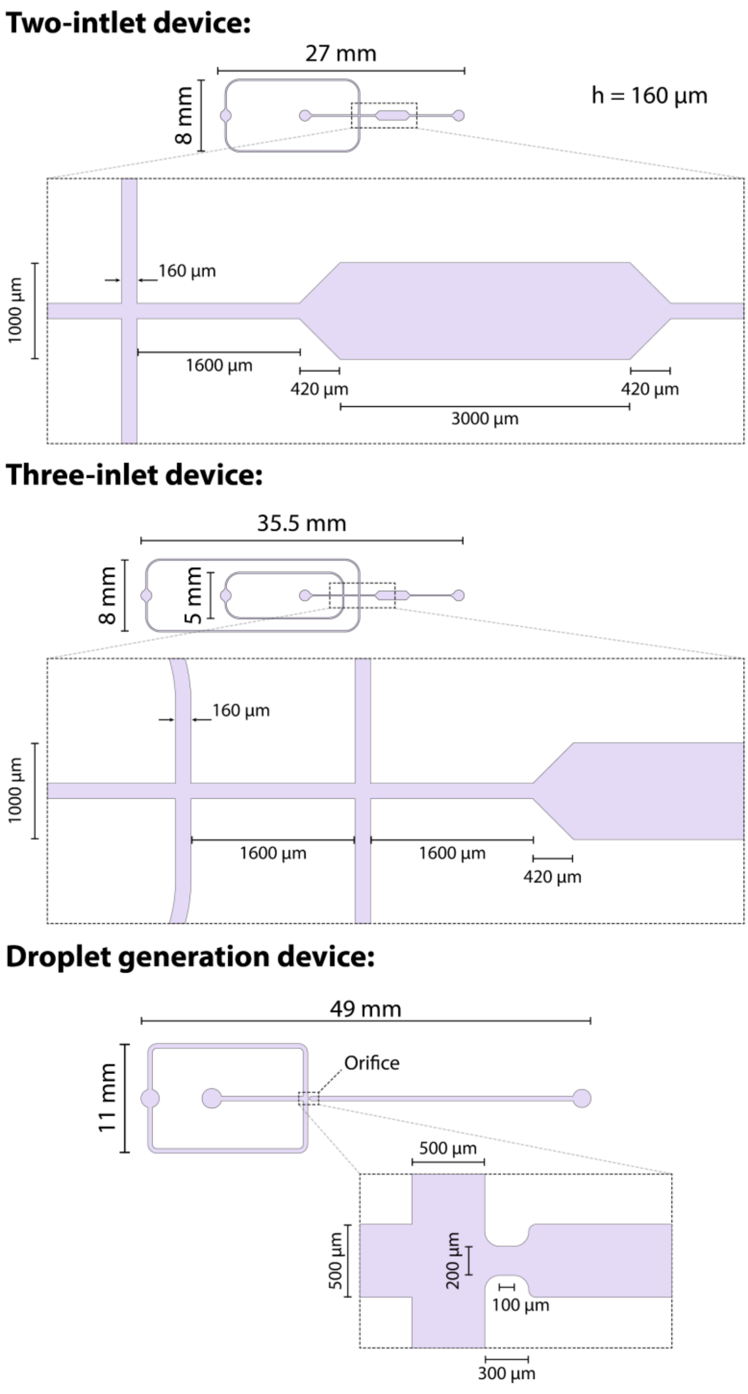

Figure S1. The geometry of the microfluidic flow focusing systems used for the generation of harmonic flow patterns when applying axial motion to the inlet tube: **(a)** Two-inlet system, **(b)** Three-inlet system. **(c)** Droplet generation system.

Supplementary information 2: Experimental setup

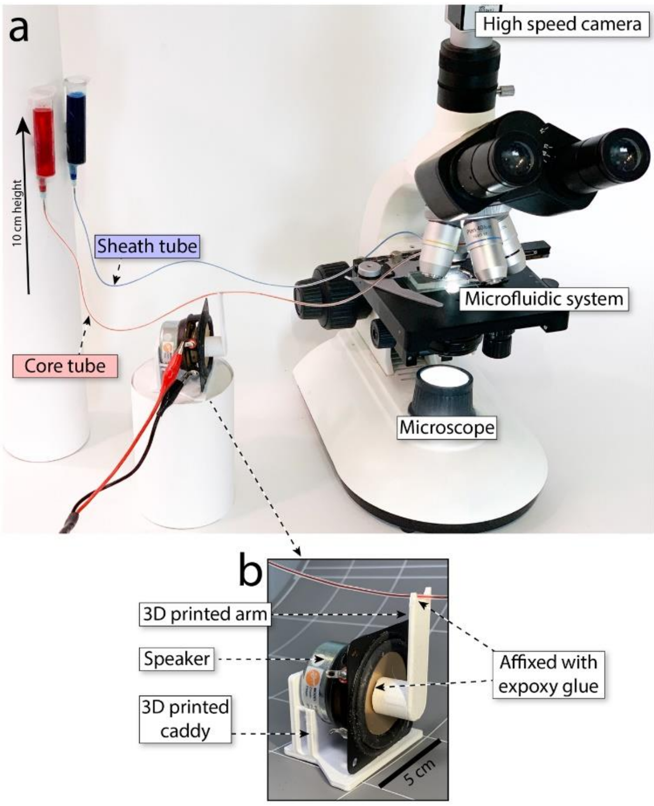

Figure S2. Photo of experimental setup

Supplementary information 3: Generation, amplification, and combination of audio signals

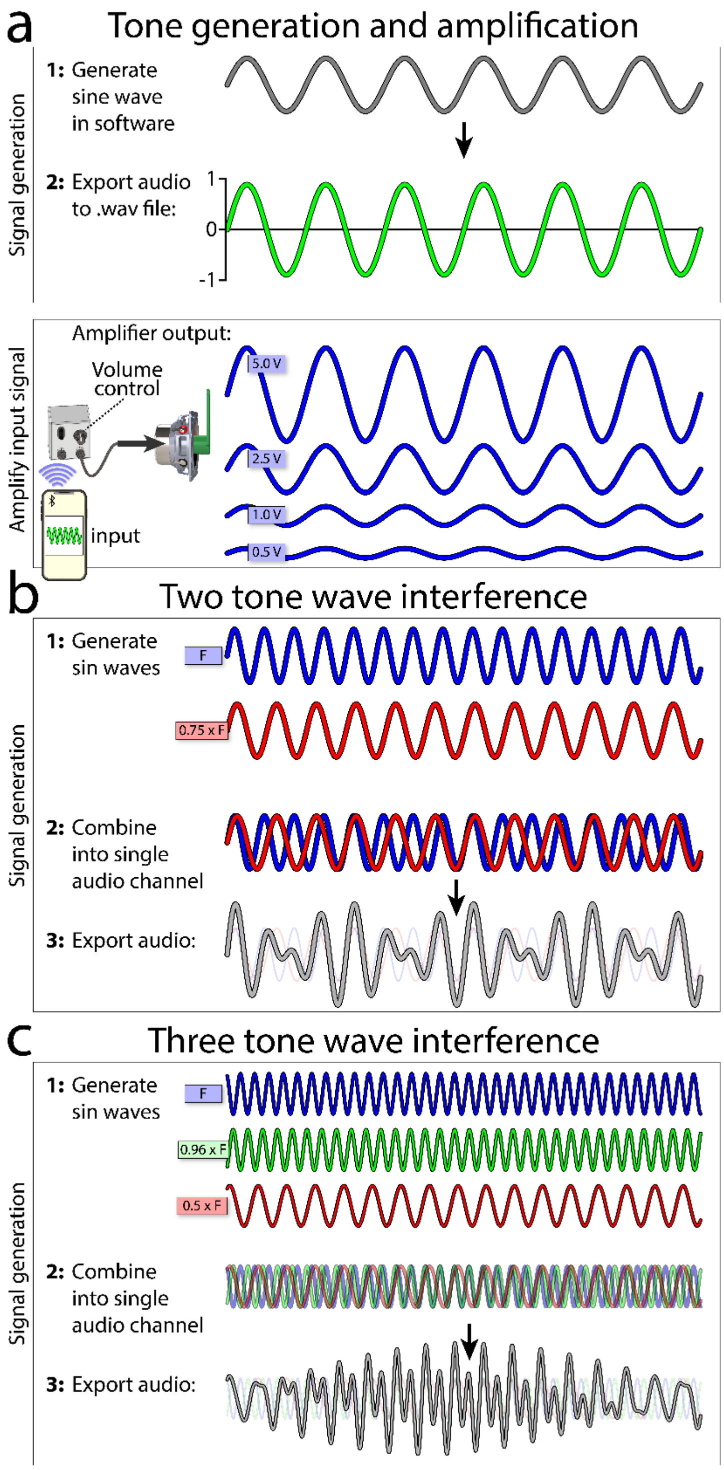

Figure S3. The procedure for generating an audio signal in software: **(a)** Generating the tone at the desired frequency, followed by exporting the tone to a digital .wav file in monoaural sound. This sound file is then amplified to the desired peak voltage and used to drive the speaker that is coupled to the microfluidic inlet tube. **(b-c)** Generation of two-tone and three-tone signals with desired frequency ratios.

Supplementary information 4: The audio spectrum of the simple piano melody

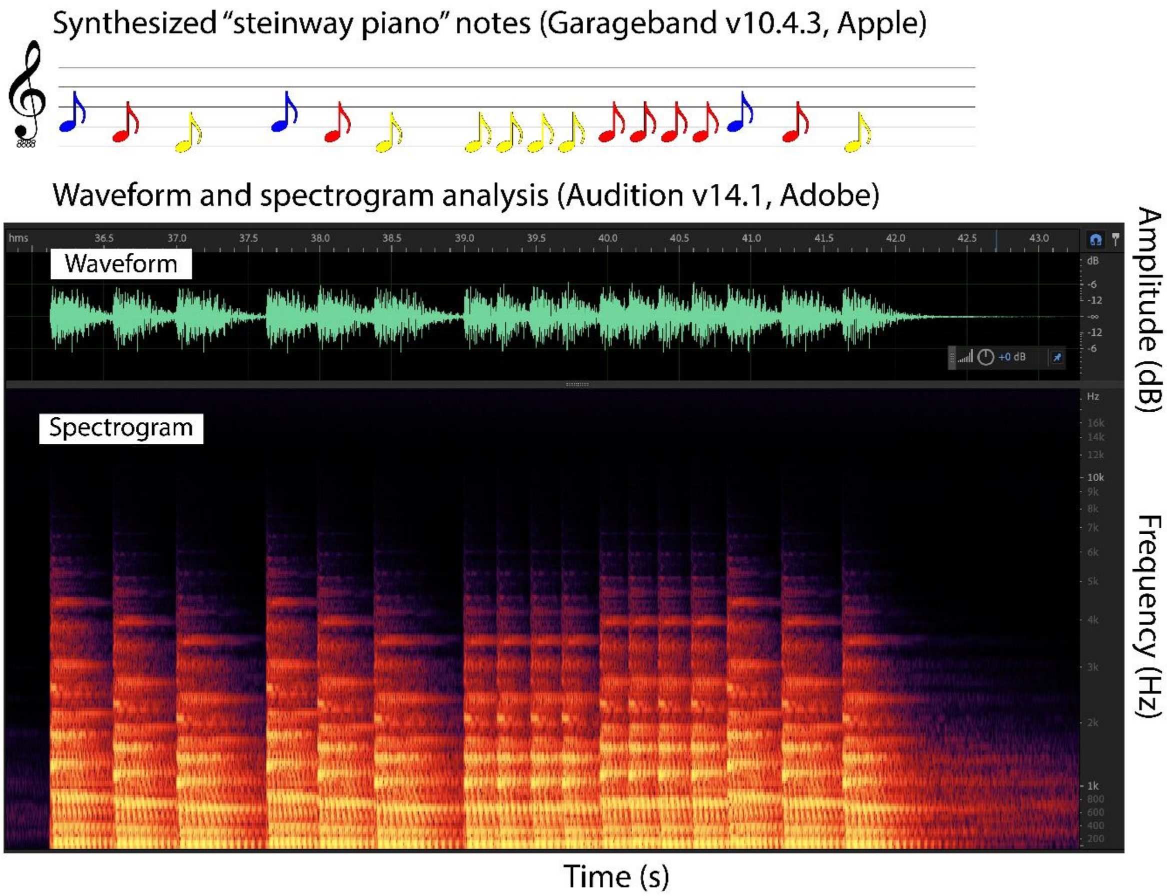

Figure S4. The audio spectrum of the simple melody, extracted from Adobe Audition

Supplementary information 5: Speaker cone displacement at various frequencies and voltages

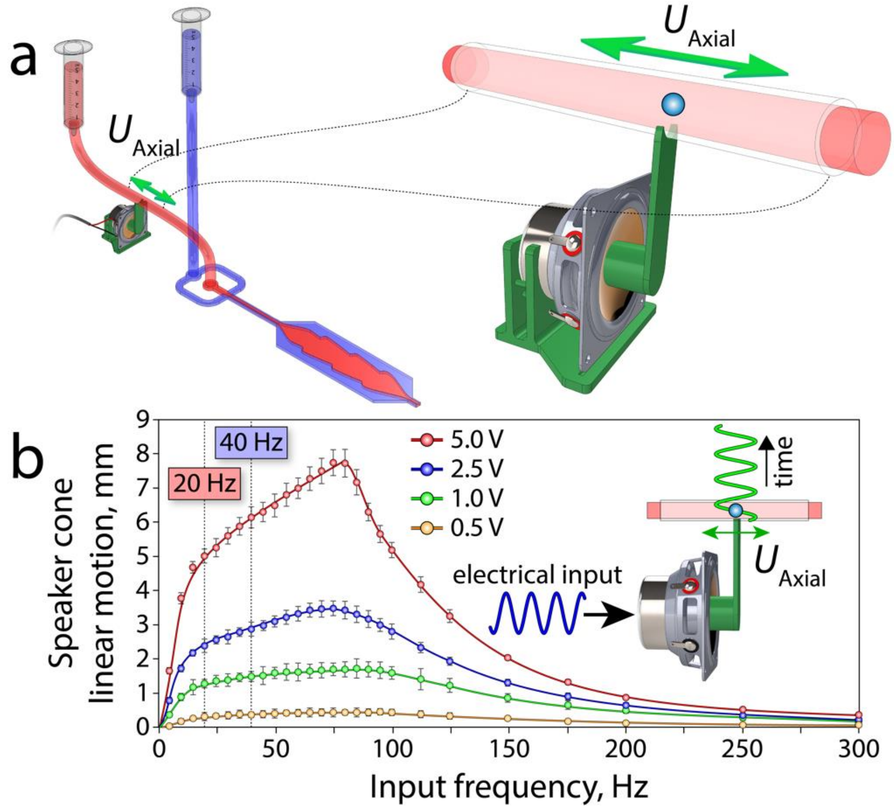

Figure S5. Characterisation of speaker cone displacement: **(a)** Experimental setup, **(b)** Variations of the speaker cone linear motion with respect to the oscillation frequency at various input voltages. Error bars correspond to average ± standard deviation obtained in three to five independent experiments.

Supplementary information 6: Numerical simulations showing the dynamic variations of the velocity profile and flow rate caused by tube axial oscillation

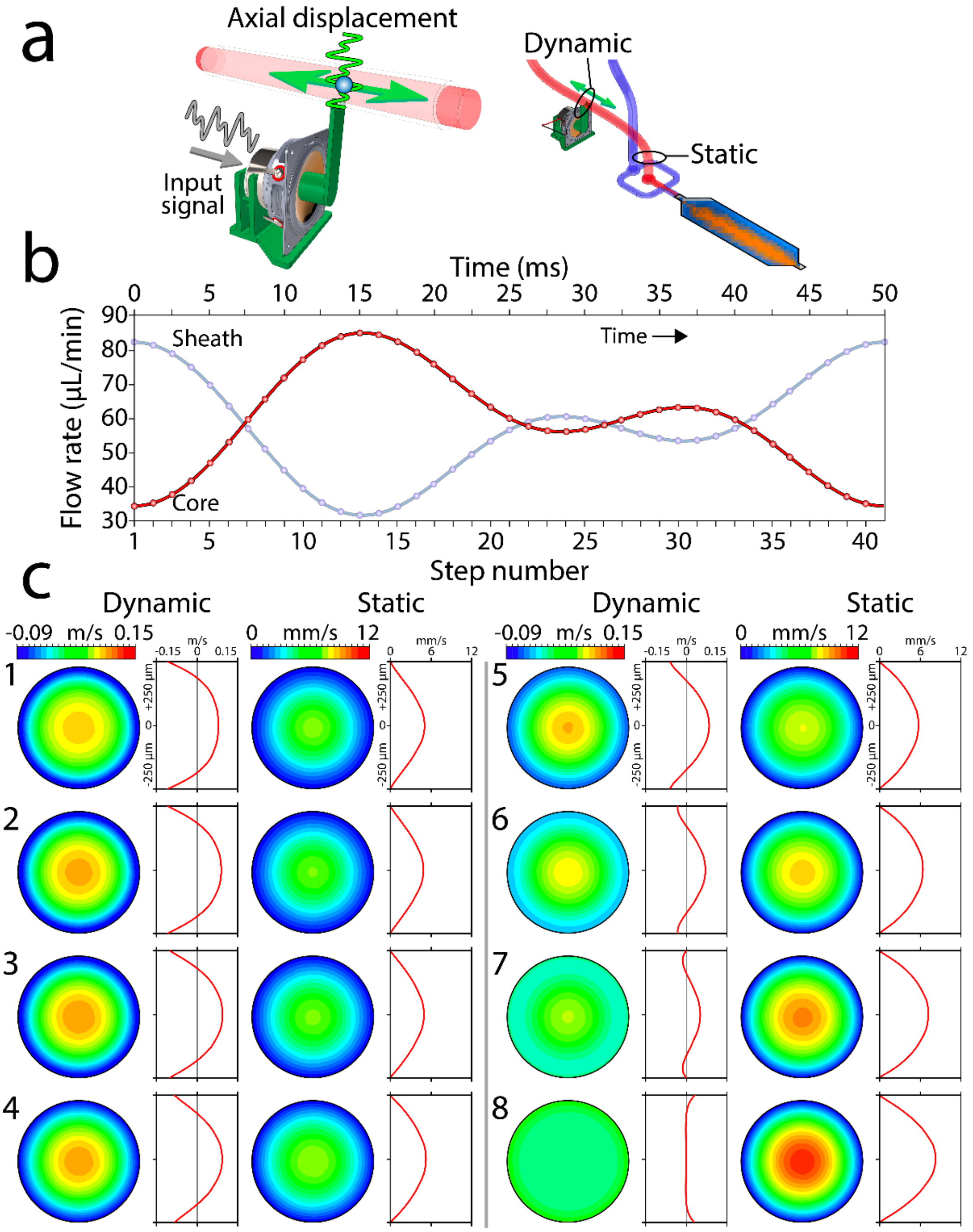

Figure S6. Numerical simulations revealing the dynamic variations of flow velocity contours and flow rate through the axially oscillating tube: **(a)** Experimental setup, indicating the dynamic (oscillating) and static segments of the inlet tube, **(b)** Dynamic variations of the core and sheath flow rates through the microfluidic system, **(c)** Variation of velocity contour and profile at the dynamic (oscillating) and static segments of the oscillating inlet tube.

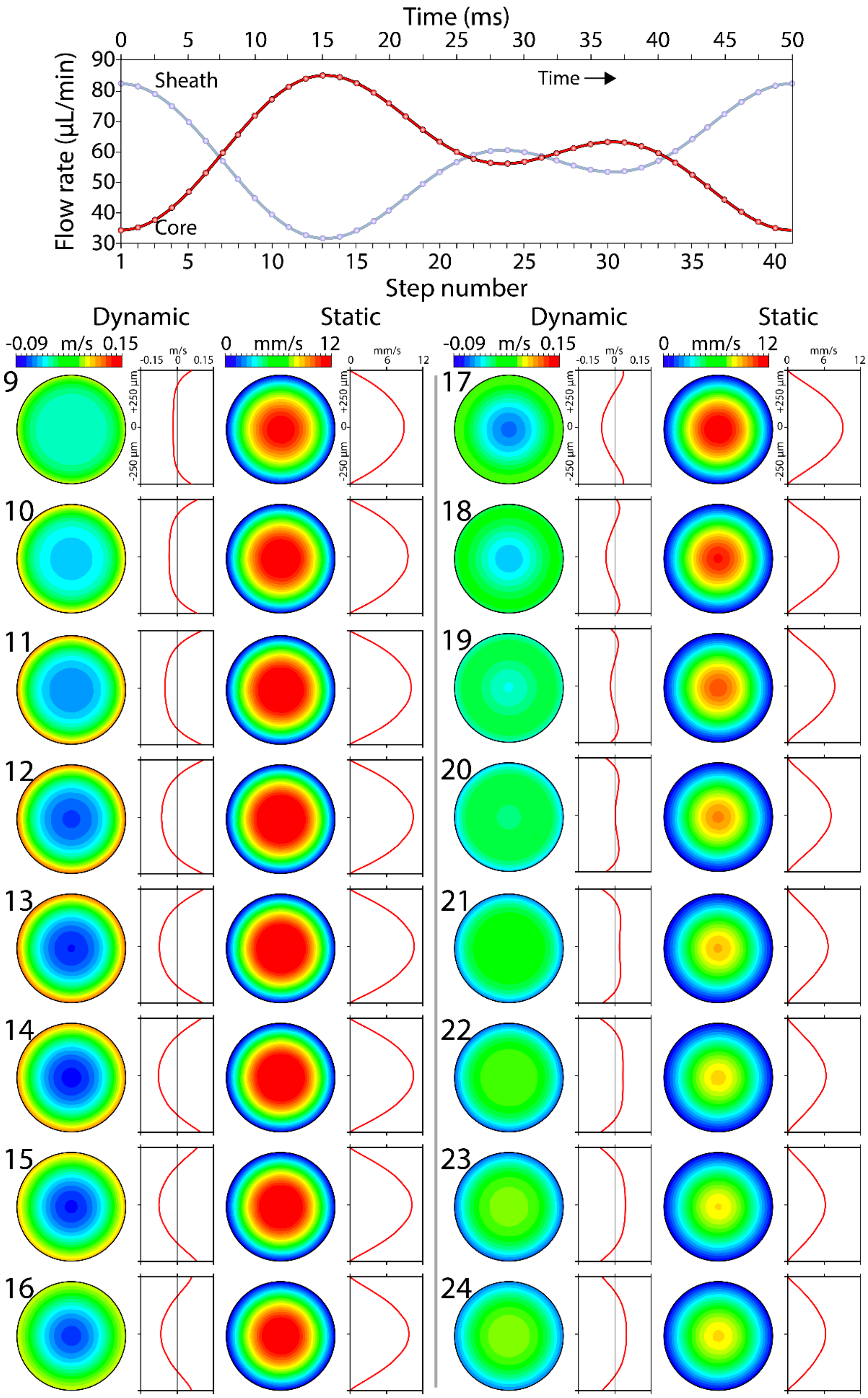

→ Continued from the previous page

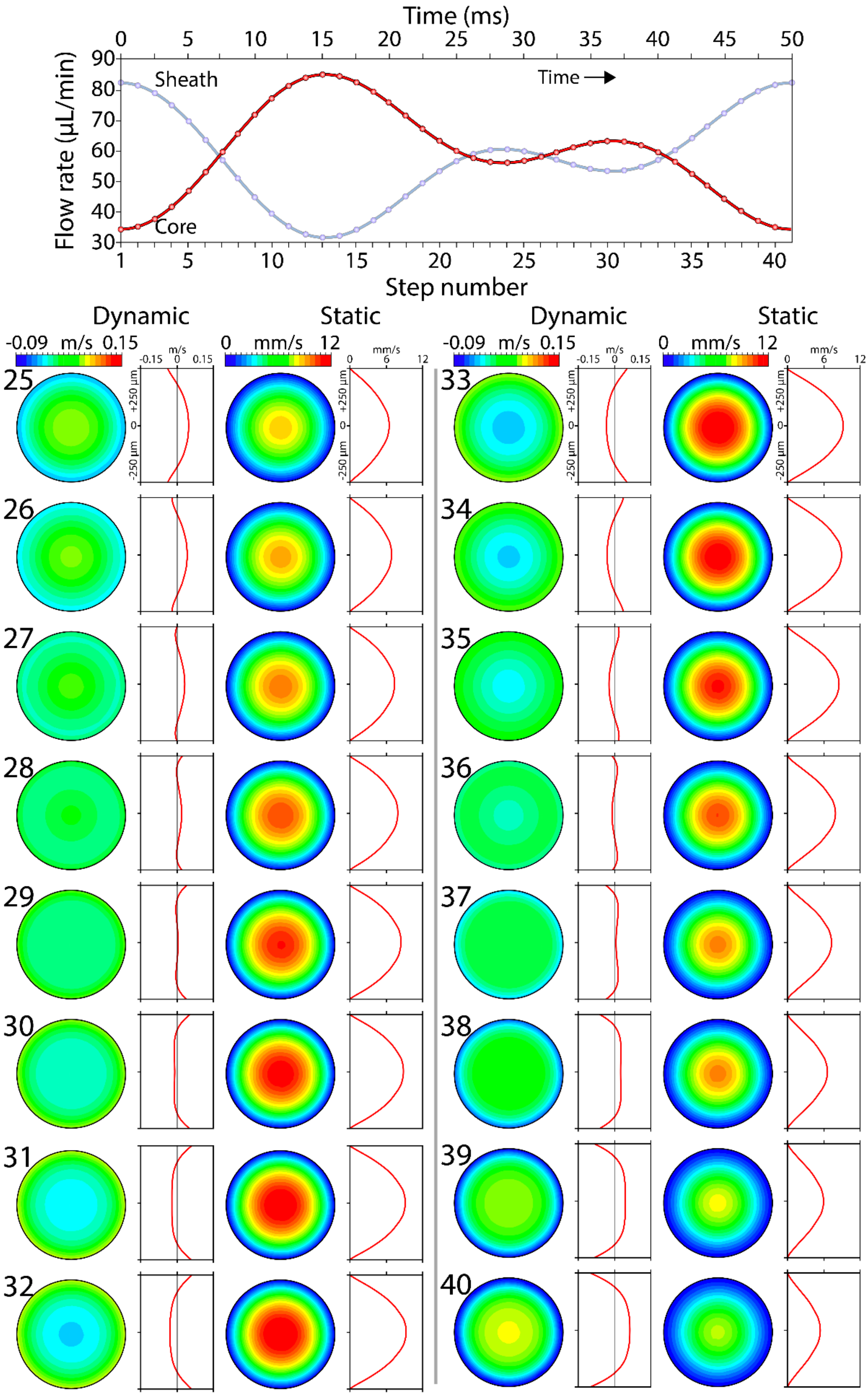

→ Continued from the previous page

Supplementary information 7: Generation of customised numbers of rib patterns by modulating the frequency ratio of two-tone signals

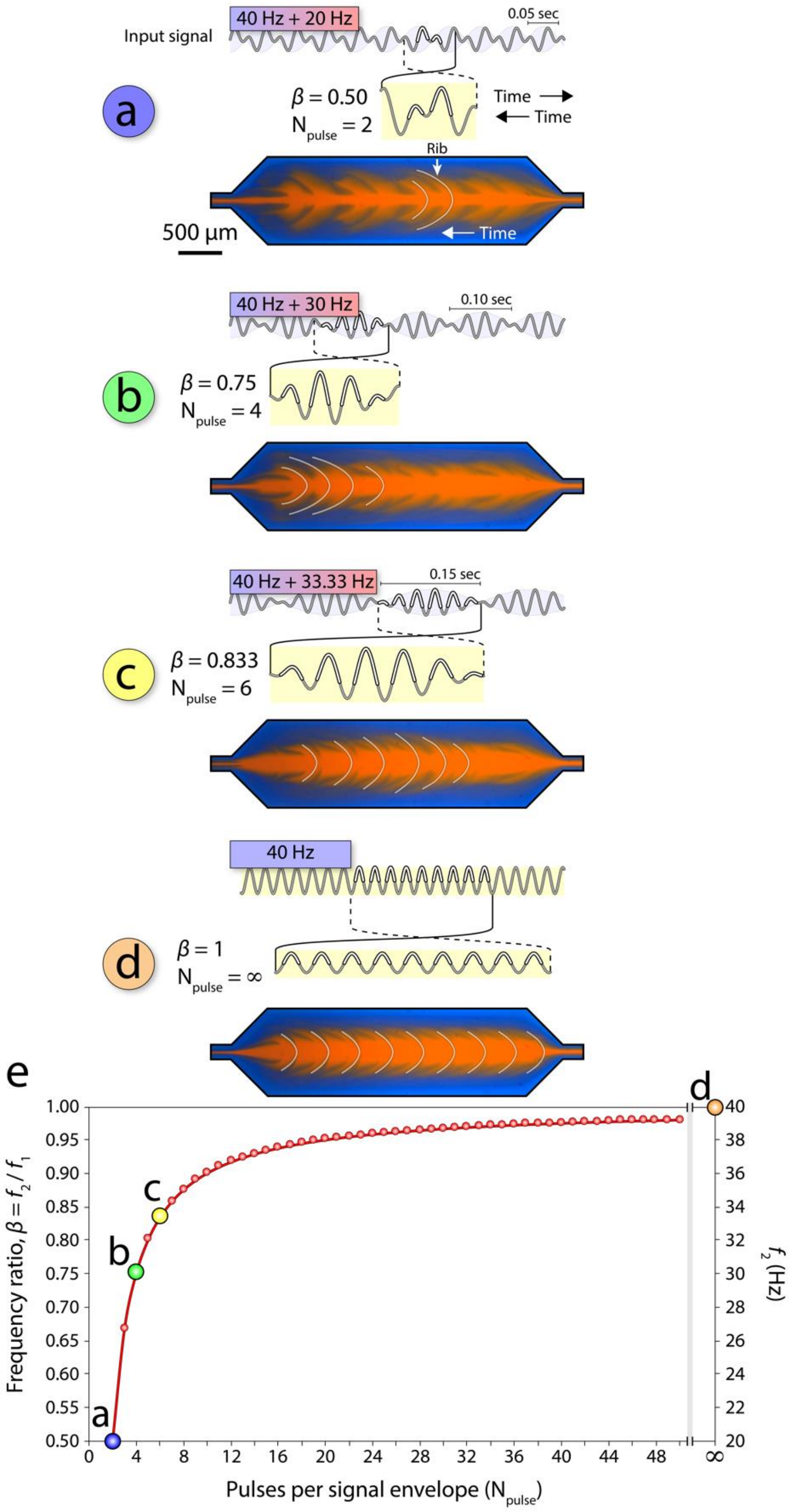

Figure S7. Customised numbers of distinct rib patterns can be generated by modulating the frequency ratio of two-tone signals: **(a)** 40 Hz + 20 Hz, $\beta = 0.5$, **(b)** 40 Hz + 30 Hz, $\beta = 0.75$, **(c)** 40 Hz + 33.33 Hz, $\beta = 0.8333$, **(d)** 40 Hz, $\beta = 1.0$, **(e)** Variations of pulses within each signal envelop against frequency ratio ($\beta = f_2/f_1$).

Supplementary information 8: Calculation of the Reynolds number of oscillating flows

$\overline{U}_{core}$ is the equivalent velocity of the core flow induced by tube oscillation was obtained by balancing the dynamic pressure caused by tube oscillation with the viscous pressure drop along the tube and the corresponding microfluidic channel:

$$\Delta P_{oscillation} = \Delta P_{viscous-tube} + \Delta P_{viscous-channel} \quad (1)$$

The dynamic pressure caused by tube oscillation is defined as: Accordingly, the viscous pressure drop along the tube and channel are defined as:

$$\Delta P_{oscillation} = 0.5\, \rho_{core} (\lambda_{tube}\, \omega_{tube})^2 \quad (2)$$

$$\Delta P_{viscous-tube} = 128\, \mu_{core}\, Q_{core}\, L_{tube} / \pi D_{tube}^4 \quad (3)$$

$$\Delta P_{viscous-channel} = a\, \mu_{core}\, Q_{core}\, L_{ch} / W_{ch} H_{ch}^3 \quad (4)$$

Step 1: Calculate the aspect ratio coefficient of the microfluidic mixing channel	$$a = \frac{12}{1 - (192\, H_{ch}/\pi^5 W_{ch}) \tanh(\pi\, W_{ch}/2\, H_{ch})} \quad (5)$$ L_{ch} : Length of the microfluidic mixing channel W_{ch} : Width of the microfluidic mixing channel H_{ch} : Height of the microfluidic mixing channel
Step 2: Calculate the equivalent dynamic flow rate of oscillating core flow	$$\overline{Q}_{core} = \frac{0.5\, \rho_{core} (\lambda_{tube}\, \omega_{tube})^2}{128\, \mu_{core}\; L_{tube}/\pi D_{tube}^2 \;+\; a\, \mu_{core}\, L_{ch}/W_{ch} H_{ch}^3} \quad (6)$$ $\overline{Q}_{core}$: Equivalent flow rate of the core flow induced by tube oscillation λ_{tube} : Amplitude of tube oscillation ω_{tube} : Angular frequency of tube oscillation ρ_{core} : Density of the core flow μ_{core} : Viscosity of the core flow L_{tube} : Length of the oscillating tube D_{tube} : Internal diameter of the oscillating tube
Step 3: Calculate the equivalent dynamic velocity of the oscillating core flow	$$\overline{U}_{core} = \frac{4\, \overline{Q}_{core}}{\pi D_{tube}^2} \quad (7)$$ $\overline{U}_{core}$: Equivalent velocity of the core flow induced by tube oscillation

Step 4: Calculate the Reynolds number of the oscillating core flow	$Re_{oscillating} = \frac{\rho_{core}\,\overline{U}_{core}\,D_{tube}}{\mu_{core}}$ $Re_{oscillating}$: Equivalent Reynolds number of oscillating flow	(8)
Step 5: Calculate the core to sheath flow viscosity ratio	$\varphi = \frac{\mu_{core}}{\mu_{sheath}}$ μ_{sheath} : Viscosity of the sheath flow φ : Viscosity ratio of core the sheath flow	(9)
Step 6: Calculate the equivalent Reynolds number in the presence of a viscosity contrast	$Re'_{oscillating} = Re_{oscillating}\,\varphi^{1.5}$ $Re'_{oscillating}$: Modified Reynolds number of oscillating flow in the presence of viscosity contrast	(10)

Supplementary information 9: Calculation of λ_{tube} and ω_{tube} for two-tone signals

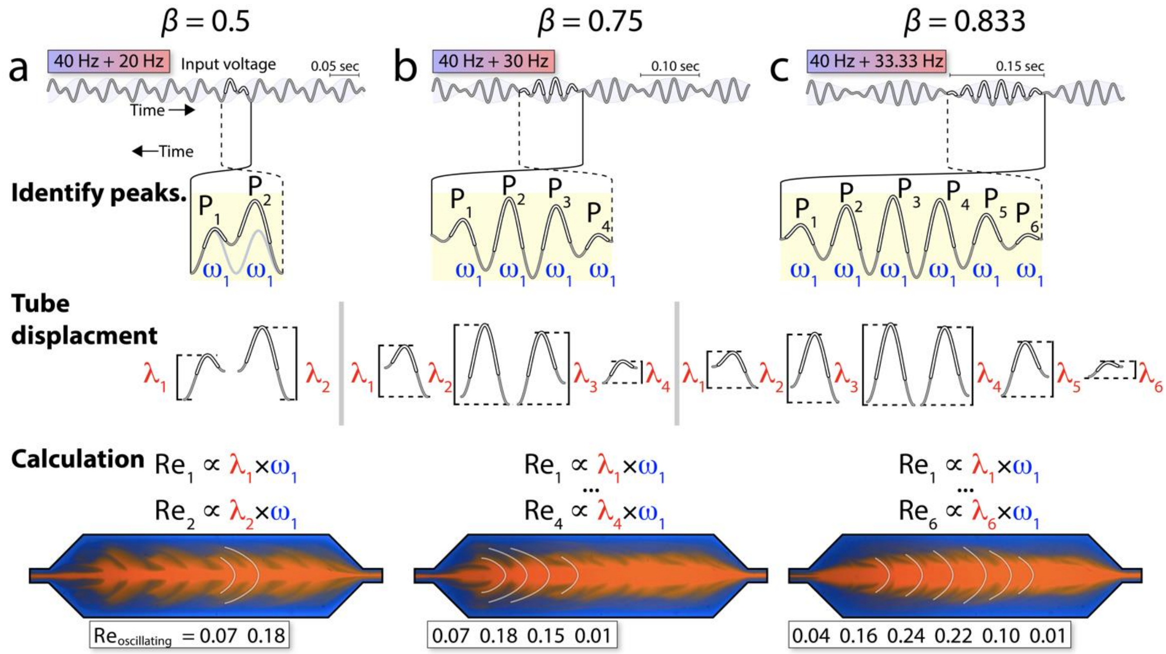

Figure S8. Calculation of λ_{tube} and ω_{tube} for two-tone signals shown for various frequency ratios of **(a)** $\beta = 0.5$, **(b)** $\beta = 0.75$, **(c)** $\beta = 0.833$. λ_{tube} is determined by the amplitude of successive pulses within a signal envelop while ω_{tube} is determined by the higher frequency.

Supplementary information 10: Transient generation of dynamic and static flow patterns using discontinuous two-tone pulses

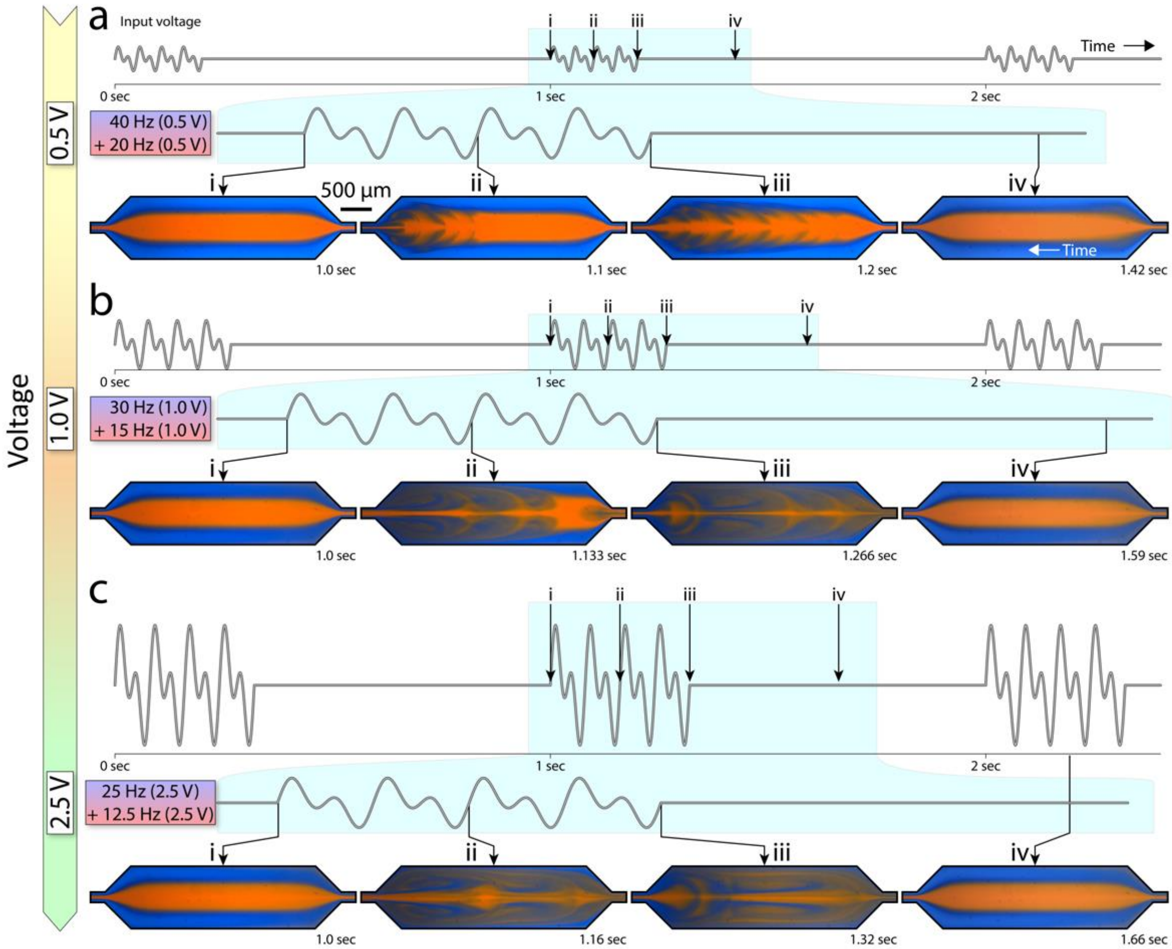

Figure S9. Generation of discontinuous dynamic flow patterns in a microfluidic flow focusing system when oscillating the core inlet tube with discontinuous two-tone signals at various oscillation frequencies and voltages applied to the audio speaker: **(a)** 20 + 40 Hz at 0.5 V, **(b)**, 15 + 30 Hz at 1.0 V, and **(c)** 12.5 + 25 Hz at 2.5 V.

Supplementary information 11: The effect of inlet tube length on the dynamics of the system

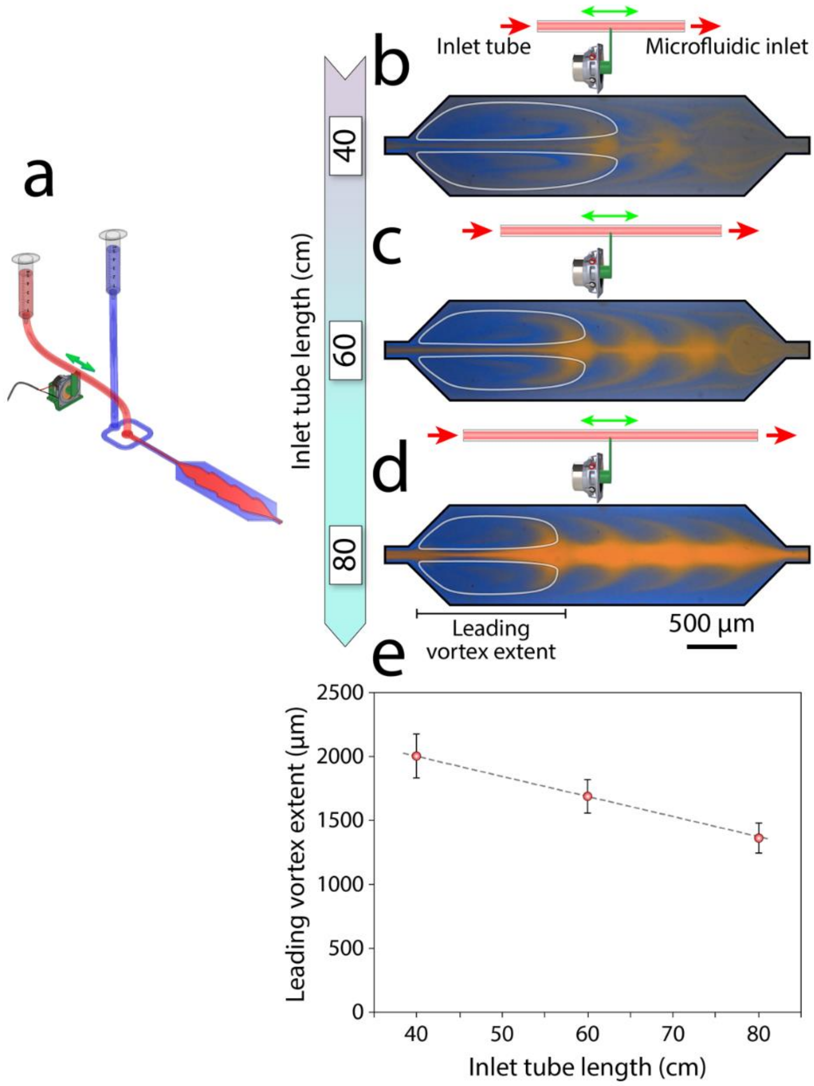

Figure S10. Studying the effect of inlet tube length on the dynamics of the system: **(a)** Schematics. **(b-d)** Snapshot images showing the extent of the leading vortex at tube lengths of 40, 60 and 80 cm. **(e)** Reduction in the extent of the leading vortex when increasing the length of the inlet tube.

Supplementary information 12: The effect of channel length on the dynamics of the system

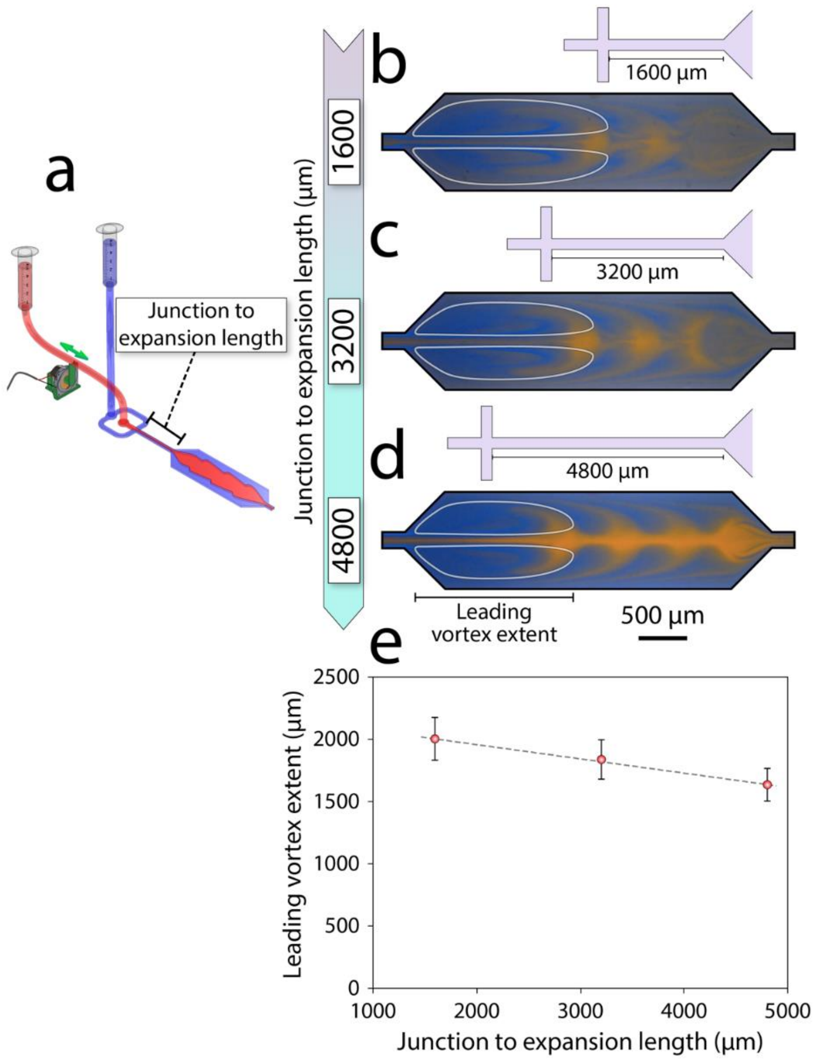

Figure S11. Studying the effect of microfluidic channel length on the dynamics of the system: **(a)** Schematics. **(b-d)** Snapshot images showing the extent of the leading vortex at channel lengths of 1.6, 3.2 and 4.8 mm. **(e)** Reduction in the extent of the leading vortex when increasing the length of the microfluidic channel.

Supplementary information 13: The effect of bulk flow rate on the dynamics of the system

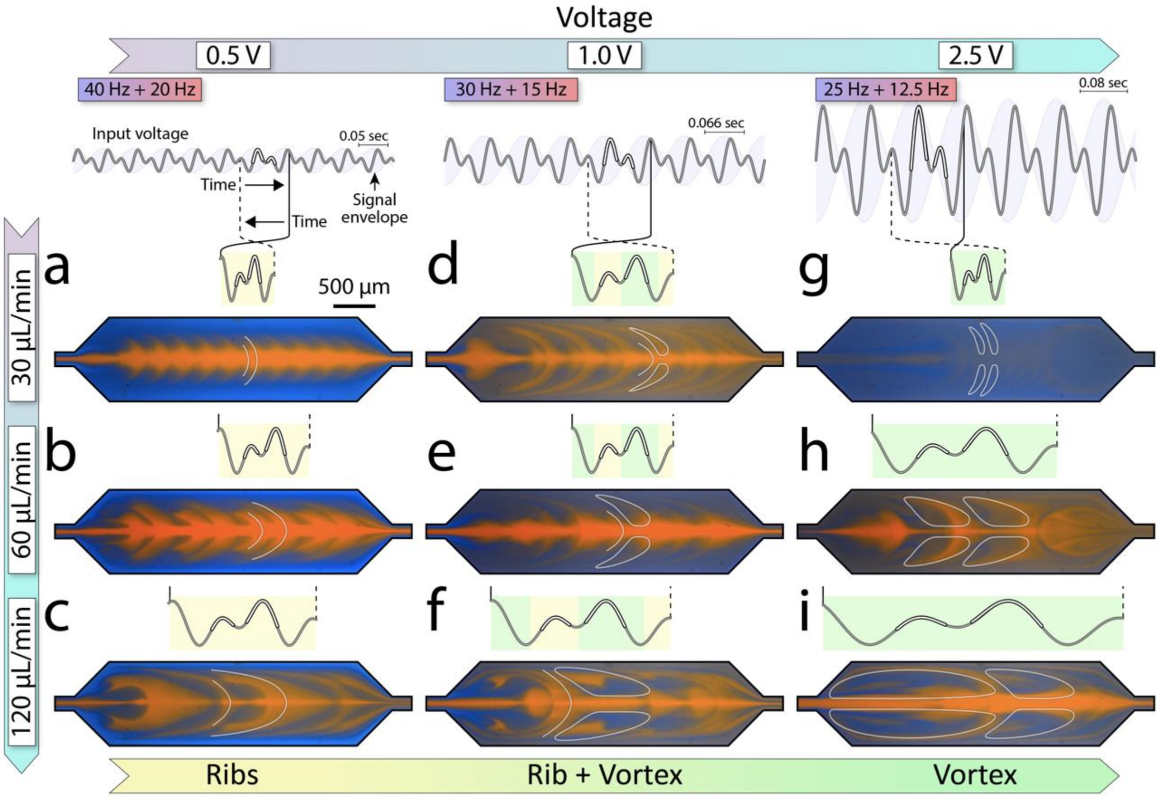

Figure S12. Studying the effect of bulk flow rate on the dynamics of the system. Results indicate the formation of rib, rib + vortex and vortex flow patterns when increasing the operating voltage of the audio speaker from 0.5 V to 2.5 V. Increasing the flow rate leads to the extension of rib and vortex flow patterns within the expansion chamber due to augmentation of inertial effects.

Supplementary information 14: Generation of complex flow patterns in a three-inlet microfluidic flow focusing system

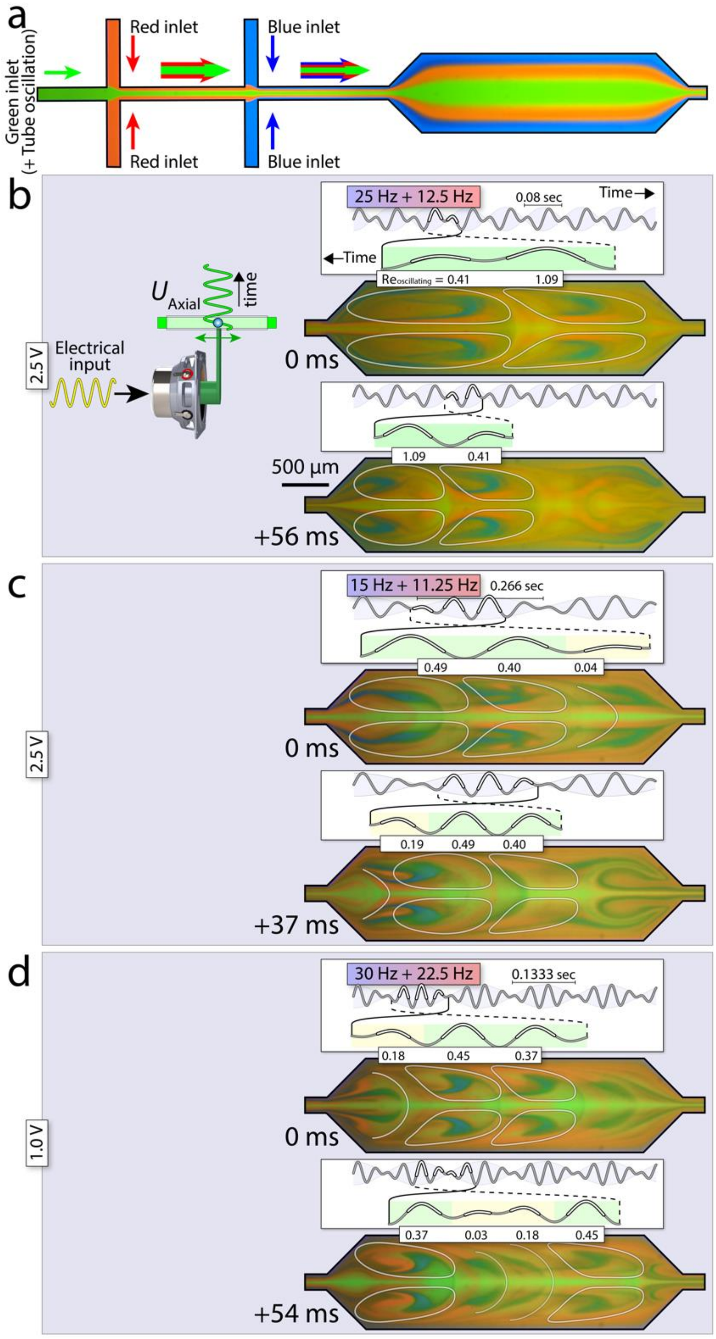

Figure S13. Generation of dynamic flow patterns in a three-inlet microfluidic flow focusing system when oscillating the core inlet tube with two-tone signals at frequency ratios of $\beta = f_2/f_1 = 0.5$ and 0.75 and various levels of the voltage applied to the audio speaker: **(a)** Experimental setup, **(b)** $V_{speaker} = 2.5$ V, **(c)** $V_{speaker} = 2.5$ V, **(d)** $V_{speaker} = 1.0$ V.

Supplementary information 15: Modulation of droplet size by axial tube oscillation

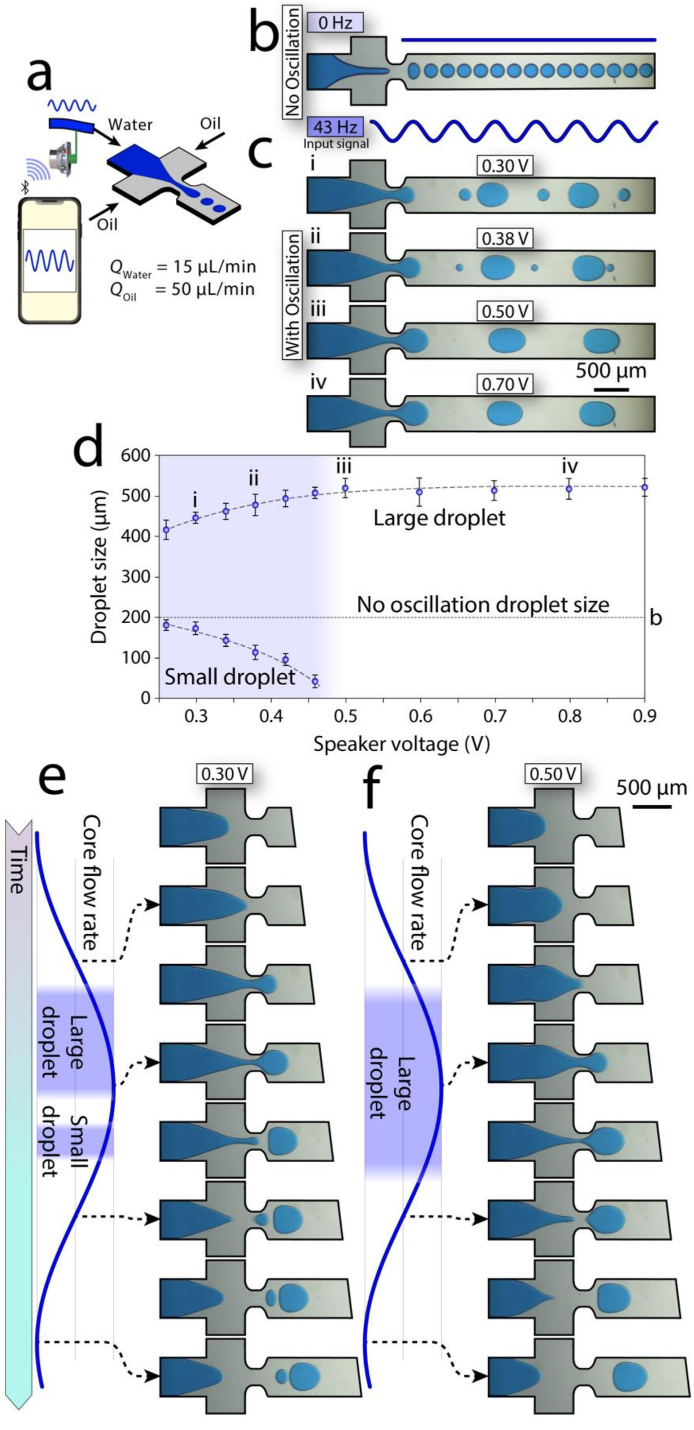

Figure S14. Tube oscillation changes the dynamics of droplet generation: **(a)** Schematics of the droplet generation setup. **(b)** Uniformly sized water droplets generated under no oscillation conditions. **(c)** Tube oscillation at 0.26-0.46 V leads to generation of a pair of small and large droplets whereas tube oscillation at 0.47-0.7 V leads to generation of only large droplets. **(d)** Variations of droplet size against speaker voltage, with error bars corresponding to average± standard deviation obtained from three independent experiments. **(e-f)** Closeup images at the orifice reveal the cyclic advancement/retraction of tapered core flow towards/from the orifice in response to dynamic changes of core flow rate.

Supplementary information 16: Generation of harmonic flow patterns in whole blood using two-tone signals (Blood sheathed by HBSS)

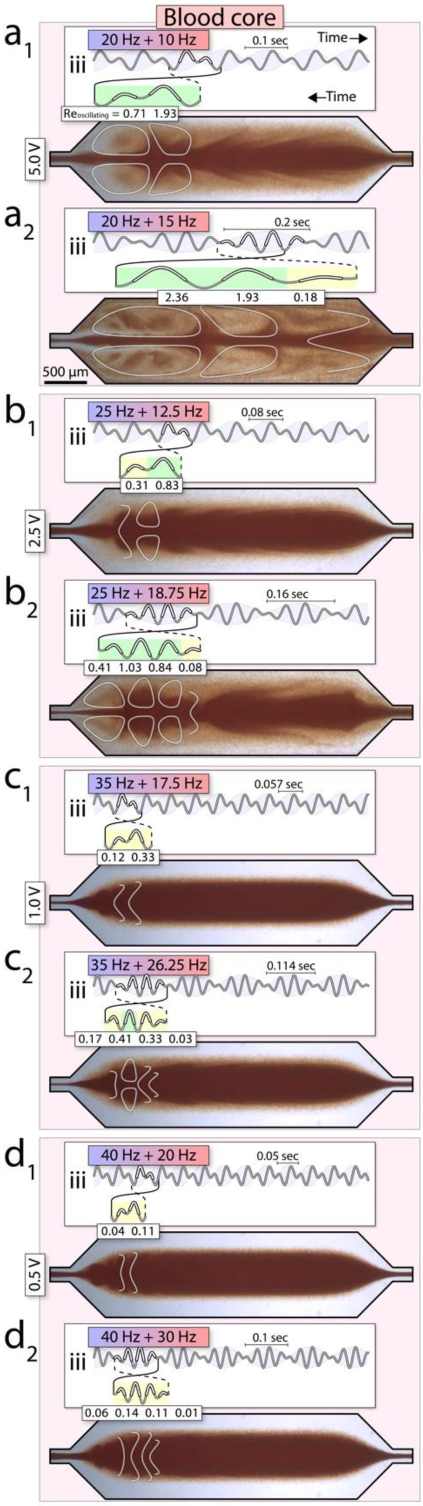

Figure S15. Generation of dynamic flow patterns when utilising the whole blood as the core liquid and oscillating the core inlet tube with two-tone signals at frequency ratios of $\beta = f_2/f_1 = 0.5$ and 0.75 and various levels of the voltage applied to the audio speaker: **(a)** $V_{speaker} = 5.0$ V, **(b)** $V_{speaker} = 2.5$ V, **(c)** $V_{speaker} = 1.0$ V, **(d)** $V_{speaker} = 0.5$ V.

Supplementary information 17: Generation of harmonic flow patterns in a viscous solution using two-tone signals

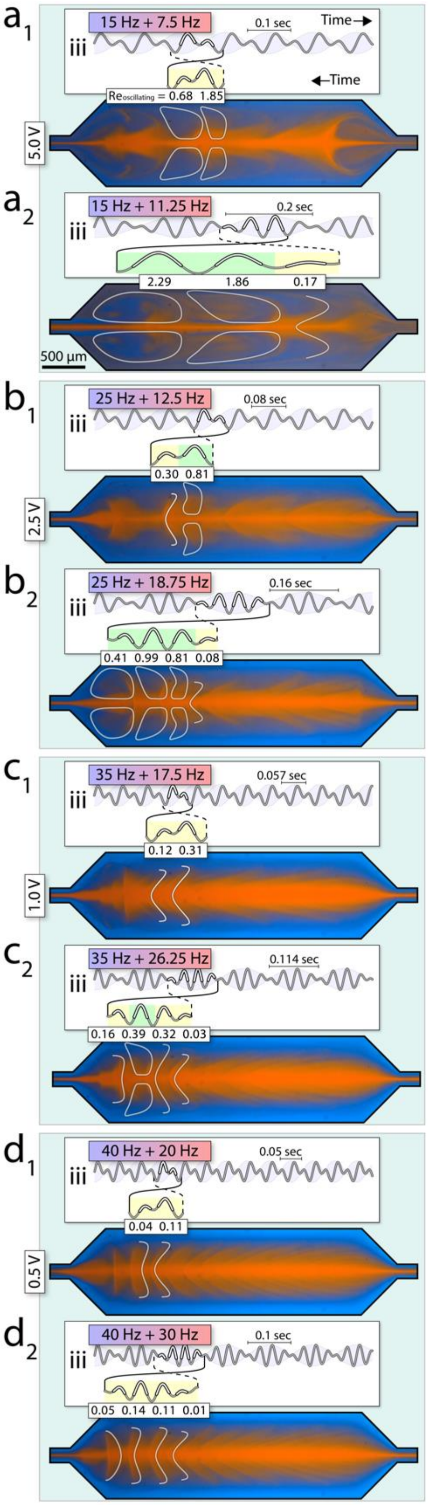

Figure S16. Generation of dynamic flow patterns at a viscosity ratio of $\varphi = \mu_{core}/\mu_{sheath} = 3$ when oscillating the core inlet tube with two-tone signals at frequency ratios of $\beta = f_2/f_1 = 0.5$ and 0.75 and various levels of the voltage applied to the audio speaker: **(a)** $V_{speaker} = 5.0\ V$, **(b)** $V_{speaker} = 2.5$ V, **(c)** $V_{speaker} = 1.0$ V, **(d)** $V_{speaker} = 0.5$ V.

Supplementary information 18: Measuring the haemolysis of red blood cells under various tube oscillation conditions

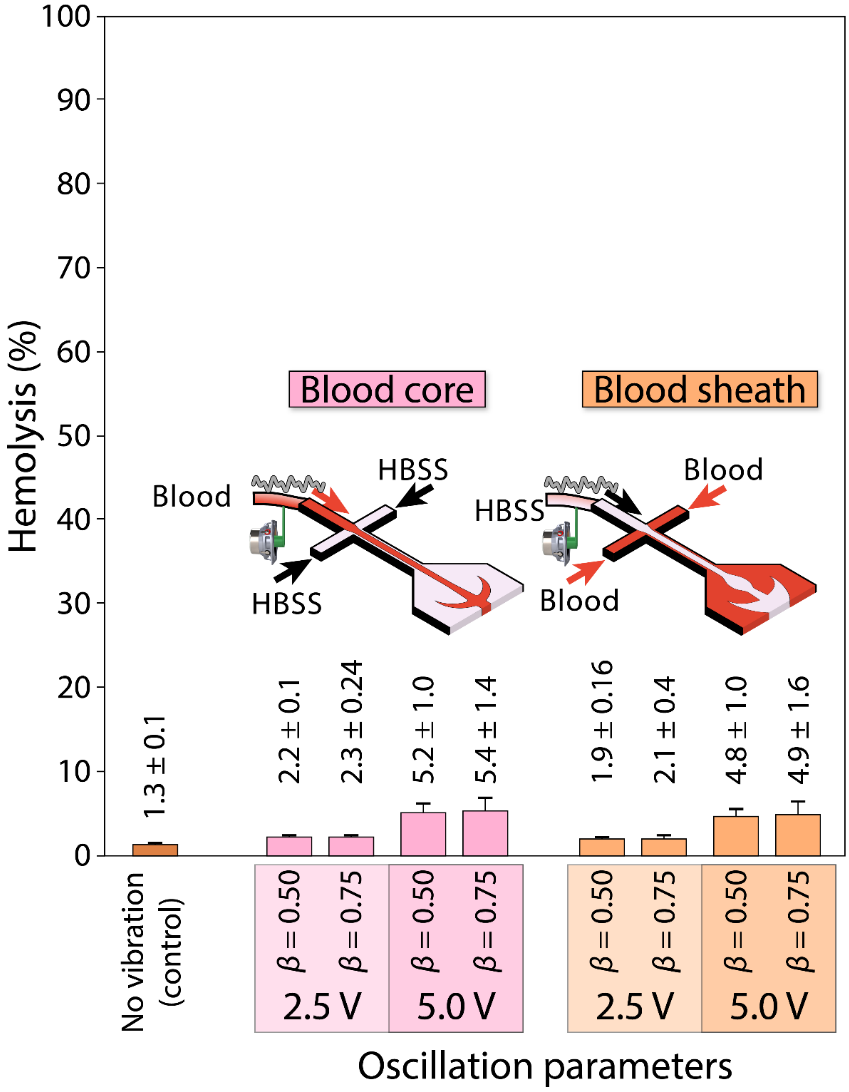

Figure S17. Haemolysis of red blood cells by analysing the haemoglobin level in cell-free plasma using a spectrophotometer under various tube oscillating conditions. Error bars correspond to average ± standard deviation obtained from three independent experiments.

Supplementary information 19: Generation of harmonic flow patterns in whole blood using two-tone signals (HBSS sheathed by Blood)

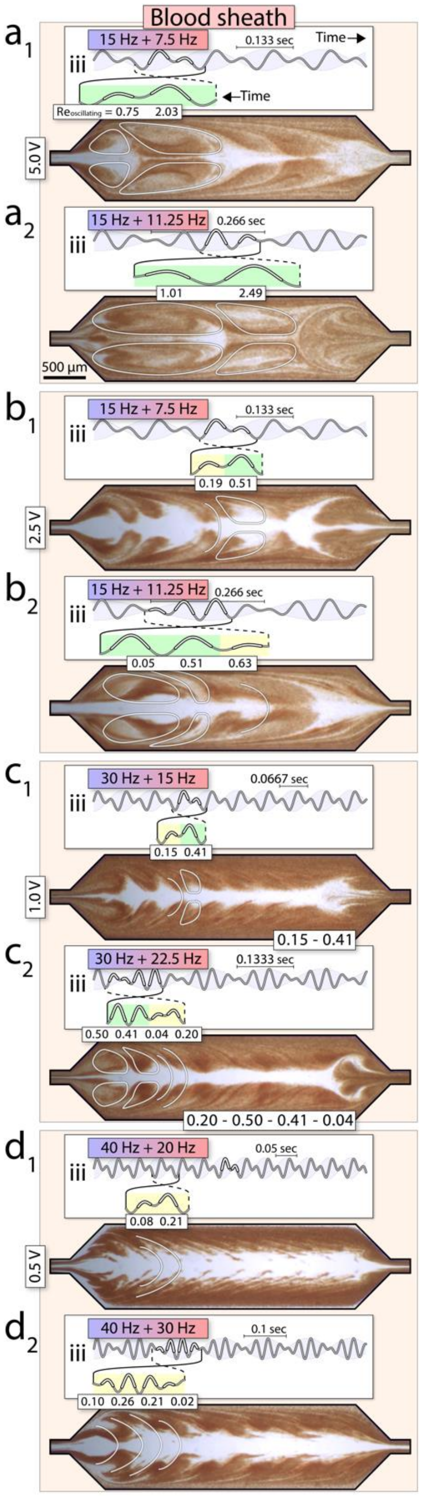

Figure S18. Generation of dynamic flow patterns when utilising the whole blood as the sheath flow and oscillating the core inlet tube with two-tone signals at frequency ratios of $\beta = f_2/f_1 = 0.5$ and 0.75 and various levels of the voltage applied to the audio speaker: **(a)** $V_{speaker} = 5.0$ V, **(b)** $V_{speaker} = 2.5$ V, **(c)** $V_{speaker} = 1.0$ V, **(d)** $V_{speaker} = 0.5$ V.

Supplementary information 20: Generation of harmonic flow patterns in water-based solutions using two-tone signals

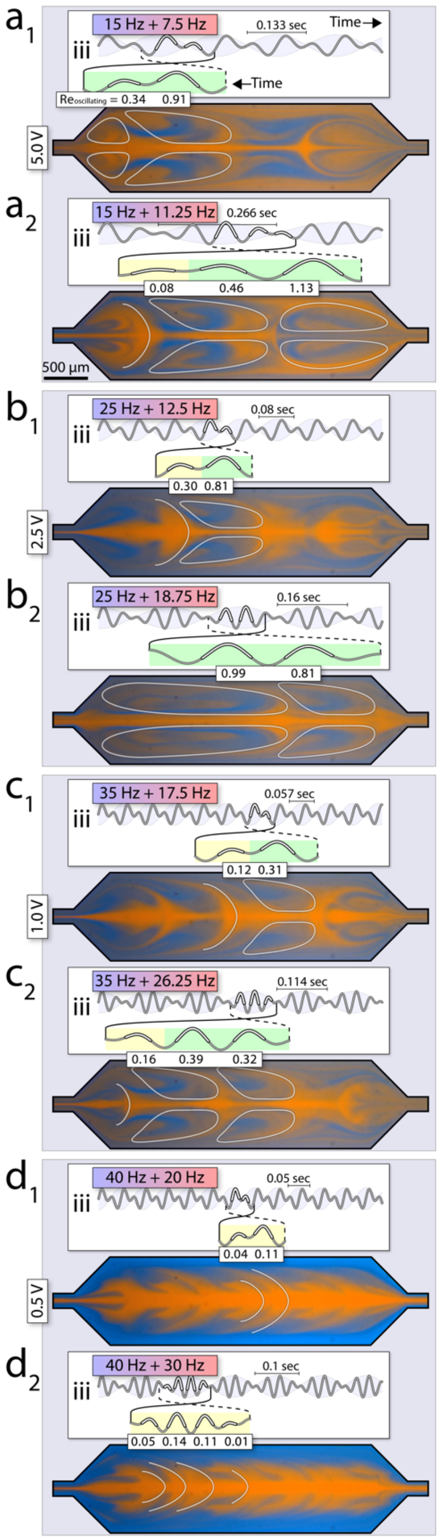

Figure S19. Generation of dynamic flow patterns when oscillating the core inlet tube with two-tone signals at frequency ratios of $\beta = f_2/f_1 = 0.5$ and 0.75 and various levels of the voltage applied to the audio speaker: **(a)** $V_{speaker} = 5.0$ V, **(b)** $V_{speaker} = 2.5$ V, **(c)** $V_{speaker} = 1.0$ V, **(d)** $V_{speaker} = 0.5$ V.

Supplementary information 21: Analysis of flow pattern map for oscillating blood flow

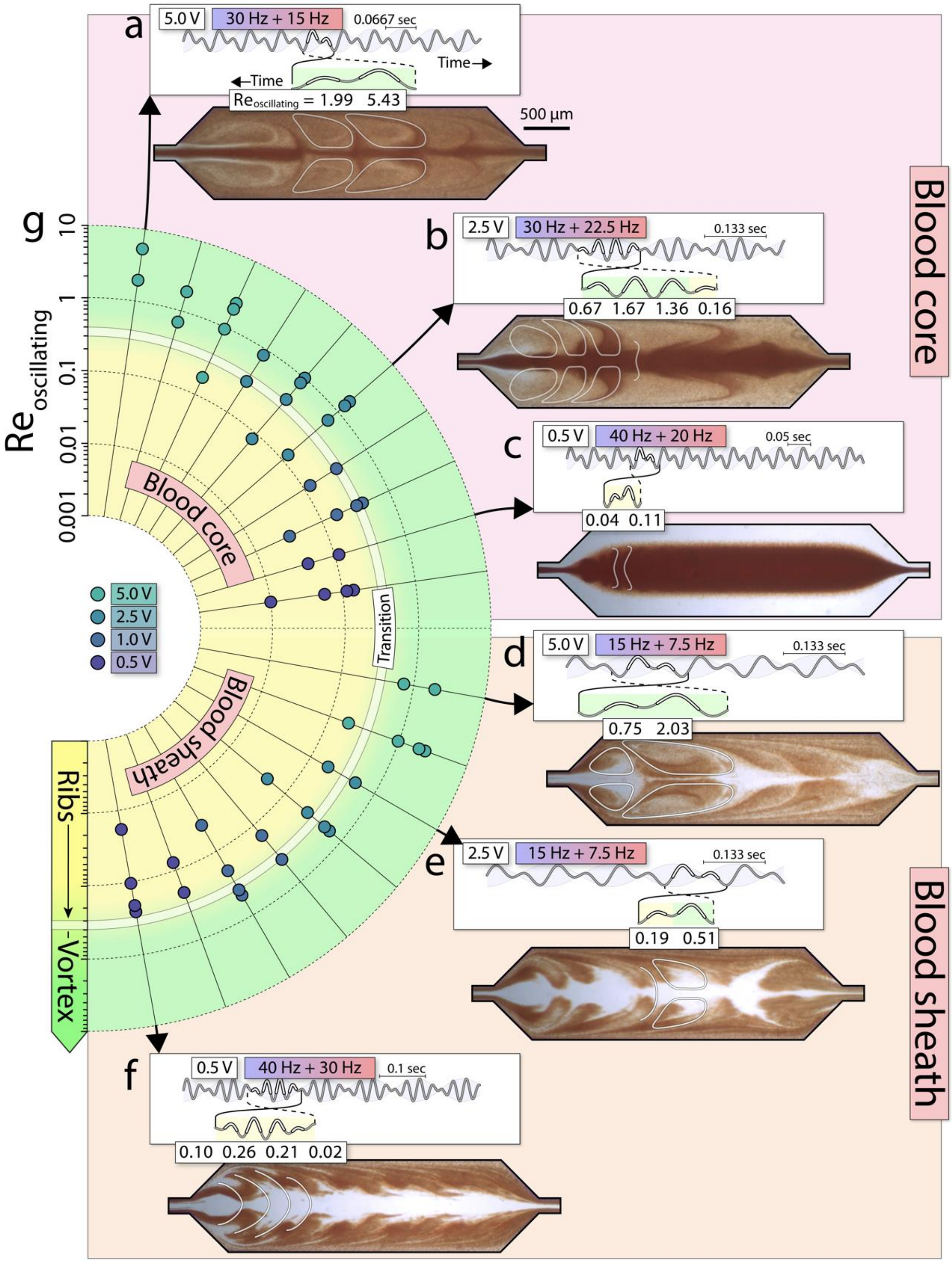

Figure S20. Flow pattern map correlating the evolution of rib and vortex patterns in whole blood to $Re_{oscillating}$ for the cases of (top) blood sheathed by HBSS and (bottom) HBSS sheathed by blood.

Supplementary information 22: Generation of harmonic flow patterns in in a water-glycerol mixture using three-tone signals

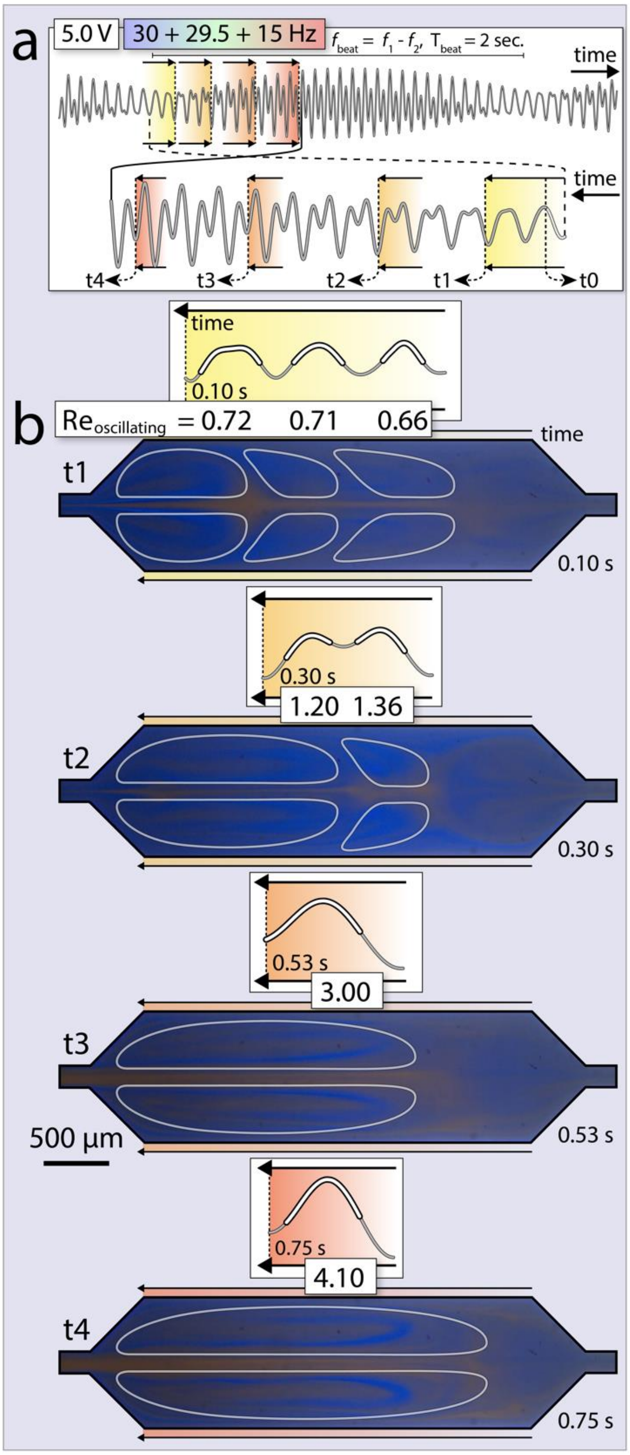

Figure S21. Generation of dynamic flow patterns in a water-glycerol mixture to resemble whole blood ($\varphi = \mu_{glycerol-water}/\mu_{water} \approx 3.5$) when oscillating the core inlet tube with a three-tone signal by combining 30, 29.5 and 15 Hz sine waves: **(a)** The three-tone waveform used for axial oscillation of the core inlet tube, **(b)** Complex vortex patterns evolved over time.

Supplementary information 23: Generation of harmonic flow patterns in water-based solutions using three-tone signals

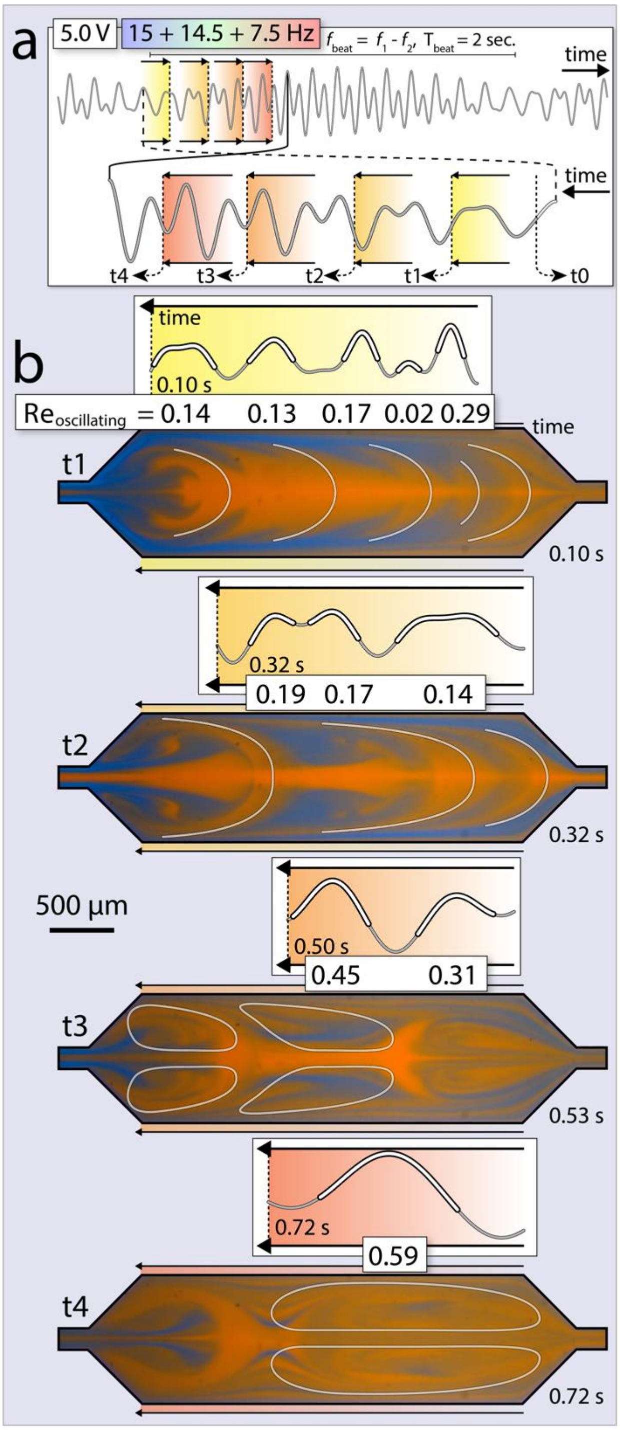

Figure S22. Generation of dynamic flow patterns in a microfluidic flow focusing system when oscillating the core inlet tube with a three-tone signal by combining 15, 14.5 and 7.5 Hz sine waves: **(a)** The generated three-tone waveform used for the axial oscillation of the core inlet tube, **(b)** Complex rib and vortex patterns evolved over time.

Supplementary information 24: Generation of harmonic flow patterns in water-based solutions using three-tone signals within a three-inlet microfluidic flow focusing system

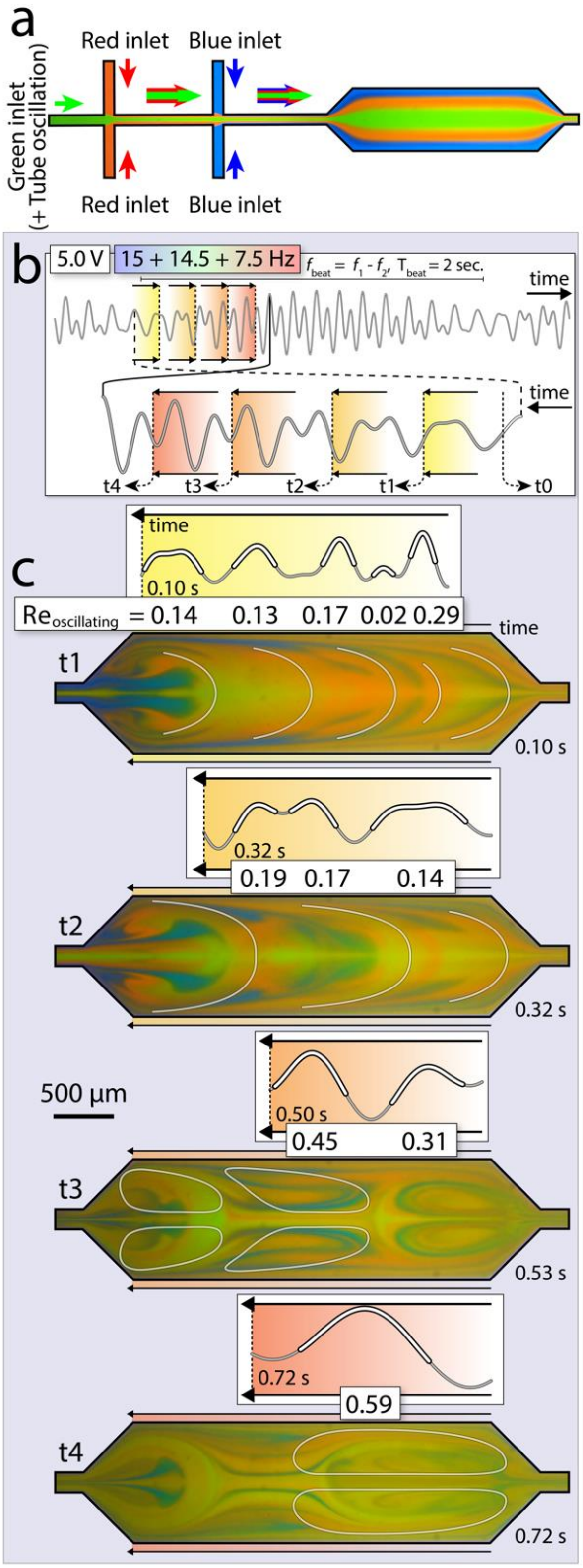

Figure S23. Generation of dynamic flow patterns in a three-inlet microfluidic flow focusing system when oscillating the core inlet tube with a three-tone signal by combining 15, 14.5 and 7.5 Hz sine waves: **(a)** The three-tone waveform used for axial oscillation of the core inlet tube, **(b)** Complex rib and vortex patterns evolved over time.

Supplementary information 25: Experimental setup for stimulation of PBMCs

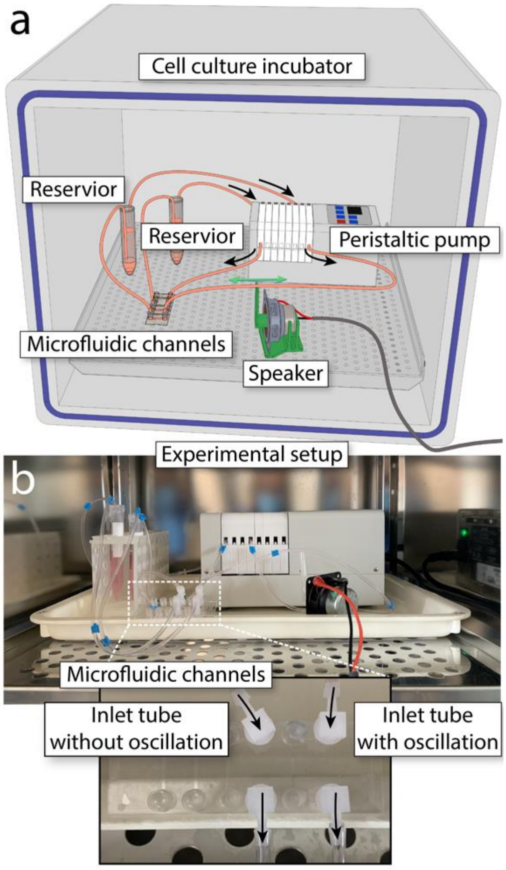

Figure S24. Experimental setup for stimulation of PBMCs: **(a)** Schematics for recirculation of PBMCs. **(b)** Actual photograph of the setup with the closeup image showing an ibidi μ-slide VI$^{0.1}$ microfluidic structure interfaced with a peristaltic pump using Tygon® tubes. The inlet tube connected to the 'with oscillation' channel is oscillated at 40 Hz using an audio speaker.

Supplementary information 26: Variations of shear rate in the oscillating inlet tube and the ibidi μ-slide VI$^{0.1}$ microfluidic channel used for stimulation of PBMCs

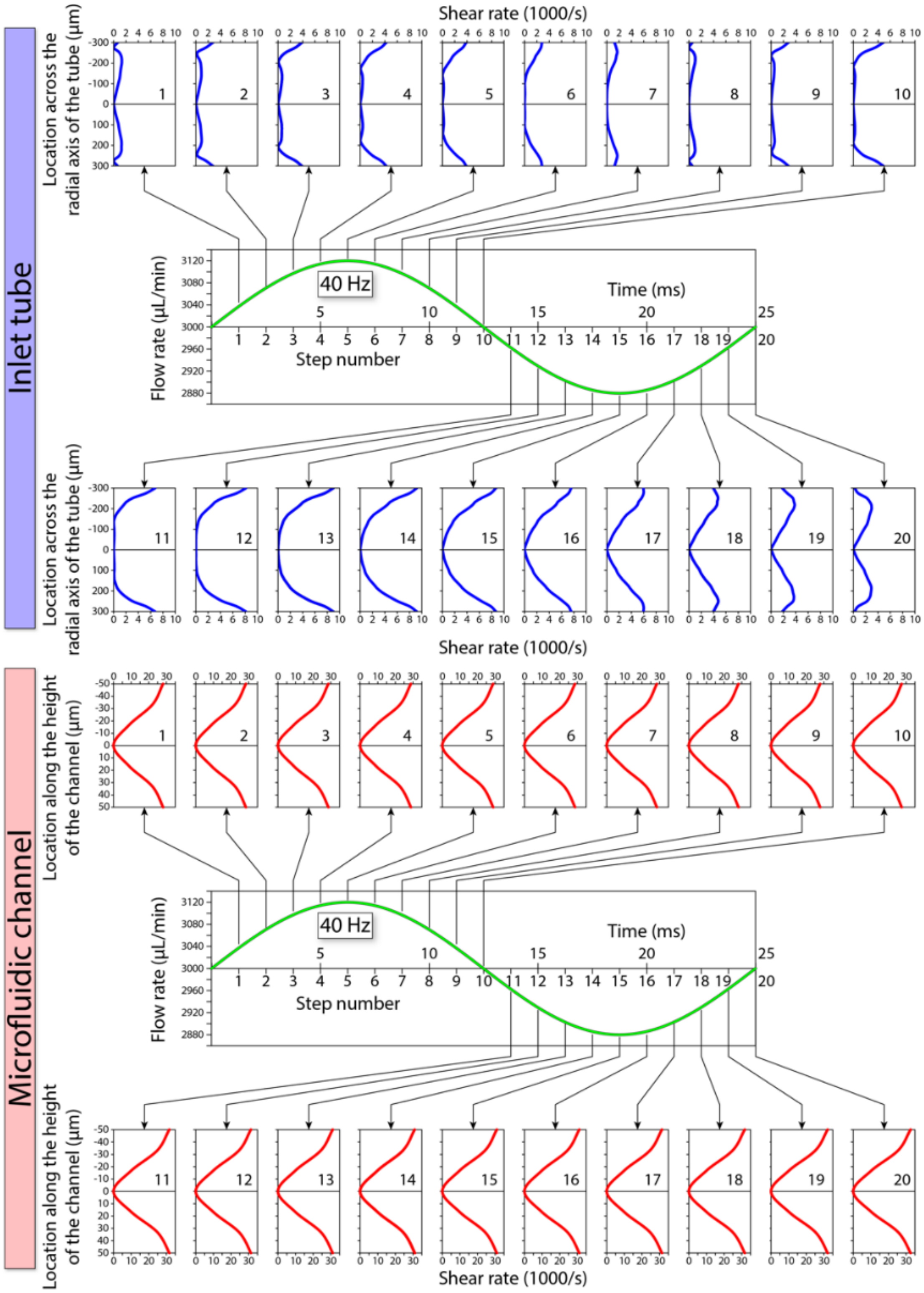

Figure S25. Variations of shear rate in the oscillating inlet tube (λ_{tube} = 1.5 mm, f_{tube} = 40 Hz) and the ibidi μ-slide VI$^{0.1}$ microfluidic channel used for stimulation of PBMCs during one cycle obtained by numerical simulations.

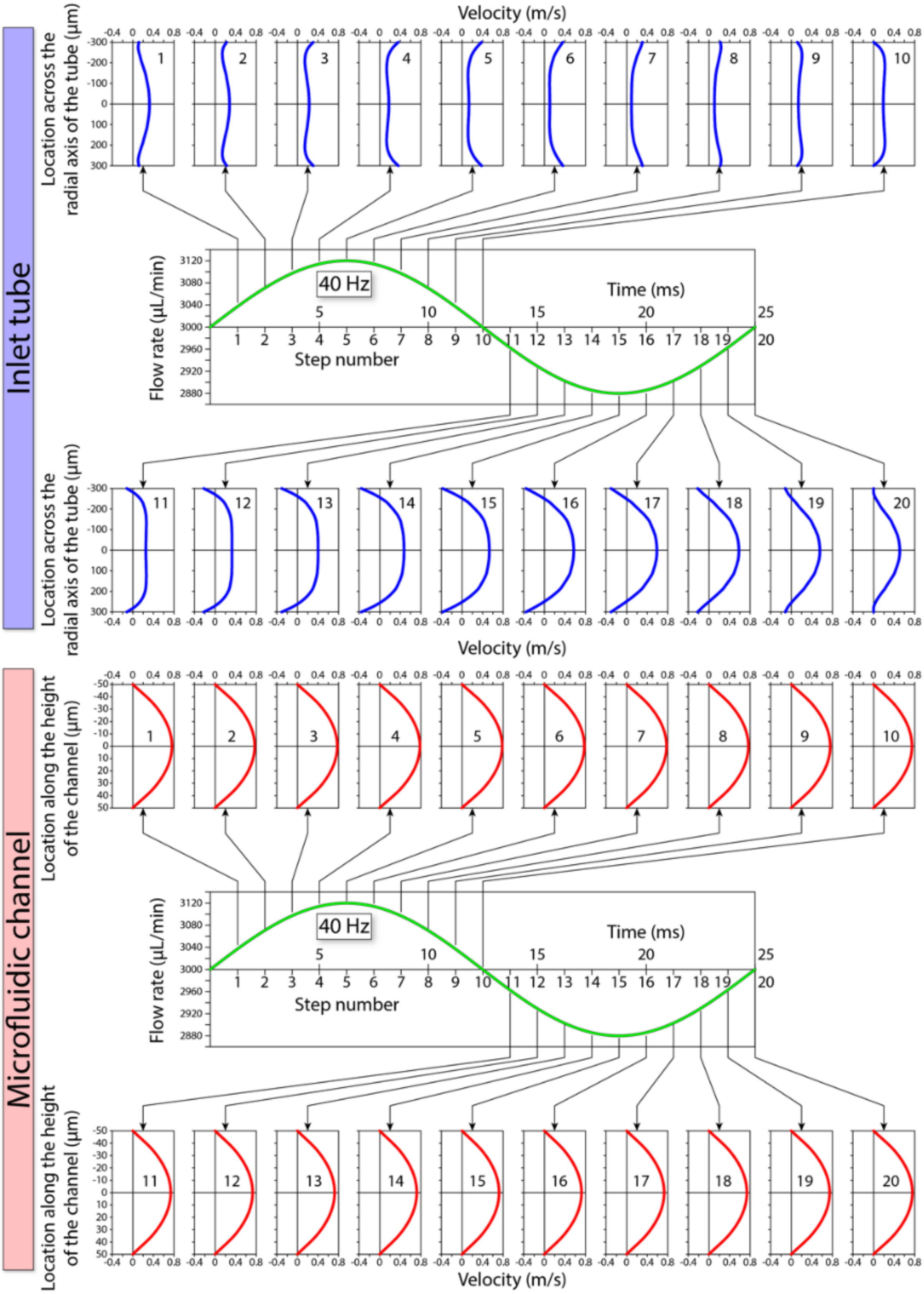

Figure S26. Variations of flow velocity in the oscillating inlet tube (λ_{tube} = 1.5 mm, f_{tube} = 40 Hz) and the ibidi μ-slide VI$^{0.1}$ microfluidic channel used for stimulation of PBMCs during one cycle obtained by numerical simulations.